Effect of temperature on Xe implantation-induced damage in 4H-SiC

C Jiang, A. Declémy, M.F. Beaufort, Alexandre Boulle, J-F. Barbot

Effect of temperature on Xe implantation-induced damage in 4H-SiC

IOP Conf. Series: Journal of Physics: Conf. Series **1190** (2019) 012015 doi:10.1088/1742-6596/1190/1/012015

Effect of temperature on Xe implantation-induced damage in 4H-SiC

C Jiang[1], A Declémy[1], M-F Beaufort[1], A Boulle[2] and J-F Barbot[1]

[1]Institut Pprime, Département Physique et Mécanique des Matériaux, CNRS-Université de Poitiers, ENSMA, BP 30179, 86962 Futuroscope-Chasseneuil
Cedex 05, France
[2]Institut de Recherche sur les Céramiques, CNRS UMR 7315, Limoges, France

E-mail: jean.francois.barbot@univ-poitiers.fr

Abstract. Damage formation in implanted 4H-SiC was studied as a function of dose and temperature of implantation. At RT the maximal strain as well as the surface swelling linearly increases suggesting a point defects swelling. With increasing temperature the slope decreases due to irradiation-induced dynamic recovery with activation energy of 0.13±0.02eV. From 300°C the amorphisation is avoided and the strain build-up can be fitted according to a direct impact model. At 300°C the as-induced strain profile consists of three different zones of damage with depth, resulting from the damage accumulation in the near surface region, the formation of Xe-vacancy complexes in the ion distribution and beyond a zone of end-of-range strain associated with interstitial accumulation.

1. Introduction

As a wide bandgap semiconductor (WBG) the 4H-SiC polytype is an attractive material especially for power devices due to their advantageous intrinsic properties. The current process for selective doping in SiC is the ion implantation. Implantation requires a post-annealing treatment to restore the crystal quality and also to achieve electrical activity of dopant. However, the growth of secondary defects or the formation of polytype structures can be observed. SiC is also a promising candidate material for advanced nuclear energy systems. Knowledge of damage accumulation under irradiation is thus important to predict the behavior of SiC under harsh environment. Whereas much effort has been devoted the study of disorder accumulation at room temperature, the effect of implantation temperature has been much less studied although this is more relevant to both applications. This paper addresses the effects of temperature in xenon-implanted SiC on the strain development and amorphization.

2. Experimental details

Single crystals of (0001)-oriented 4H-SiC were implanted with 180 kV-Xe^{3+} at various temperatures ranging from RT to 800°C in a large range of fluences up to 10^{16} $Xe^{3+}cm^{-2}$. For the low temperature runs, i.e. where the amorphous transition takes place, the current density was fixed at 0.4 $\mu A.cm^{-2}$ to minimize any additional temperature effects. The dose in displacement per atom (dpa) was obtained by a conversion factor [10^{15} $Xe^{3+}cm^{-2} \cong 3$ dpa at the maximum of the nuclear energy profile] calculated using SRIM code [1] with displacement energies of 20 and 35 eV for C and Si atoms, respectively.

The distribution of incident Xe-ions is of Gaussian shape with a mean projected range R_p~145nm and straggling ΔR_p~35nm. On the contrary the distribution of nuclear energy losses is strongly left-skewed with a mean range R_D<100nm.
At RT part of the target was masked during the implantation and the resulting step height (surface swelling) was measured by using a scanning interferometer. The ion-induced elastic strain was measured by means of X-ray diffraction (XRD) measurements conducted in the Bragg coplanar geometry with the Cu-Kα_1 radiation (more detail in [2]). Because of Poisson expansion induced by the rigid unirradiated part of the crystal, the actual strain due to the damaged zone is only 84% of the total measured strain [3,4]. XRD simulations were also performed to determine the strain profile [5]. Cross-sectional transmission microscopy (XTEM) specimens were prepared by focused ion beam (FIB), and TEM images were conducted on a JEOL2200FS.

3. Results and discussion

Figure 1(a) shows the XRD curves of 540 keV Xe-implanted 4H-SiC at 200°C up to 1.2 dpa (4x10^{14} Xe.cm^{-2}). All the curves show the Bragg peak due to the unperturbed bulk diffraction and, at lower angles a tail of scattered intensity increasing with fluence. This scattering tail induced by implantation results from a dilatation gradient of the lattice along the normal direction [6]. As observed in figure 1, the maximum strain given by the position of the last fringe, increases with increasing fluence. At the highest fluence the disappearance of fringes and the low diffracted intensity suggest that the onset of amorphization transition (in the range 0.6-1.2 dpa). At this level of damage a continuous buried amorphous layer is indeed observed by XTEM (figure 1b) while a layer containing dark contrast spots are observed at lower fluences (figure 1c) in the highly damaged region.

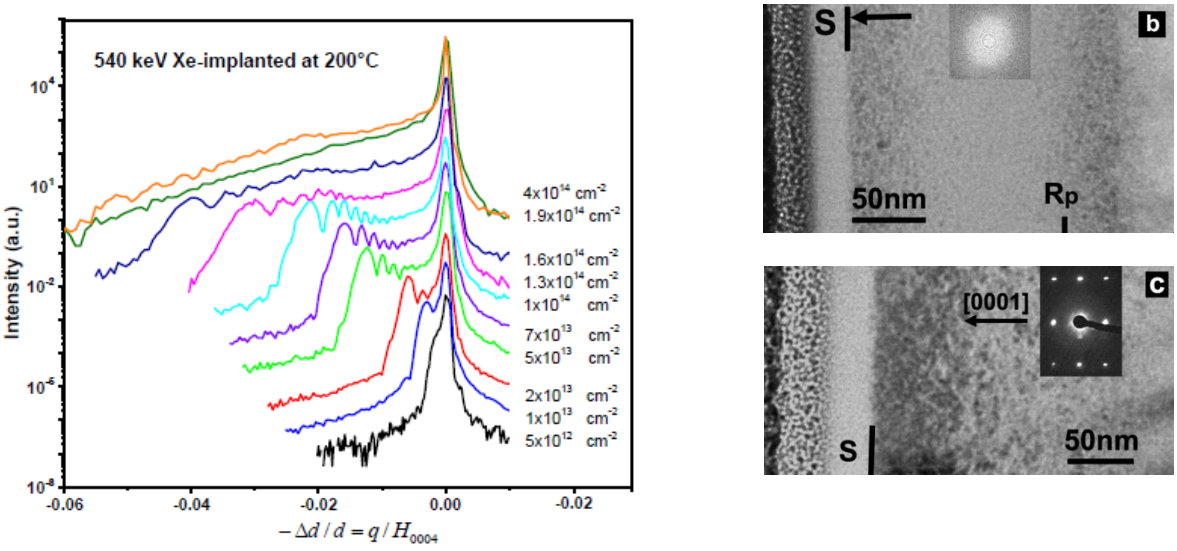

Figure 1. Left: evolution with increasing fluences of the X-ray scattered intensity distribution along the surface direction close to the (0004) reflection of SiC implanted with 540 keV xenon ions at 200°C (Δd/d) is the normal strain- Right: XTEM images of SiC implanted at 1.2 dpa (b) and 0.6 dpa (c)

Figure 2 shows the evolution of the maximal strain at RT, 200, 250 and 300°C as function of the dose. For temperatures lower than 300°C the maximal strain linearly increases up to amorphization. The slope of the line decreases with increasing temperature of implantation, from ~17%.dpa^{-1} at RT to 5-6%.dpa^{-1} at 250°C suggesting an increase of dynamic recovery with temperature as reported in Al-implanted SiC [7]. At RT the step height, h, also varies linearly indicating a point defect swelling regime, and the step height only results from the elastic strain given by:

$$h \sim h_e = \int_0^\infty \varepsilon(z) dz \approx \varepsilon_{max}.R_p \quad (1)$$

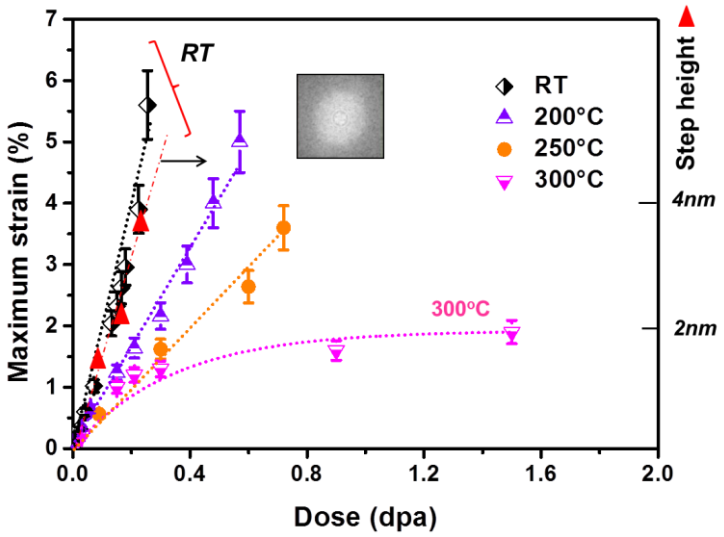

Figure 2. Dose dependence of the maximal strain at different temperatures in Xe-implanted 4H-SiC. At RT the step height, *h*, has also been measured.

From figure 2 the threshold amorphization doses versus temperature were estimated. The results were fitted using a dose-temperature relationship to describe the temperature dependence of the amorphization threshold, given by [8,9]:

$$\emptyset_{c/a} = \frac{\emptyset_0}{1 - Ke^{-E_a/kT}} \quad (2)$$

where the pre-factor K was taken as $K = 1/\sigma_{eff.}.\emptyset$, $\sigma_{eff.}(T)$ being the effective capture cross section for strain accumulation. Assuming that only the irradiation-induced recovery processes are operative in this temperature range, the activation energy for the dynamic recovery processes, E_a , is found to be 0.13±0.2 eV in good agreement with the one found in MeV Xe^+ irradiated 6H-SiC [8]. However, in contrast with [8] the temperature at which amorphisation is avoided, is shifted to higher temperature ($250<T_{a/c}<300$°C) of implantation. This could come from dose rate effects, unless the damage efficiency increases with the incident ion energy [10]. At 300°C there is a balance between generation and recombination which can be well described by a direct impact (*DI*) model in the investigated range of doses that can be expressed as:

$$\varepsilon_{max}(T) = \varepsilon^{sat}(T)\left[1 - \exp(-\sigma_{eff.}.\emptyset\right] \quad (3)$$

With increasing temperature up to 800°C, the *DI* model is still operative (equation (3)) and only the level of strain at saturation is temperature dependent, $\varepsilon^{sat}(T)$, with activation energy $E_a = 80 \pm 10\ meV$, determined from an Arrhenius plot. This activation energy is similar to the one previously determined from subsequent annealing [2, 11] and may be attributed to the recombination of point defects due to long-range migration. On the contrary the effective cross section for strain buildup is no more temperature dependent suggesting a unique process of strain accumulation at elevated temperature. The saturation of strain in this temperature range suggests a saturation of surface swelling as reported in Kr-implanted SiC at elevated temperature [12]. With increasing dose a second step of strain was evidenced showing that other mechanisms can operate [2].

Figure 3 shows experimental and simulated θ-2θ scans from 4H-SiC implanted with xenon ions at 300°C and different doses. The corresponding depth-profiles of elastic strain were determinate from the simulations of the XRD curves using the RaDMaX software (continuous lines). At low dose the strain depth profiles are bell-shaped and localized close to the mean projected range of damage in agreement with SRIM calculations. With increasing dose, the maximal strain continuously increases

and shifts toward the bulk. At high doses the strain distribution is clearly bimodal with a maximum close to the damage maximum, R_D, and a deeper one localized around R_p. This clearly shows that the implanted xenon plays a predominant role on the vacancy-type defect stability as predicted by DFT calculations [13]. An end of range strain also appears with increasing dose, up to 350nm approximately. Subsequent annealing should promote different kinds of defects according the different zones. This is reported in Kr-implanted 3C-SiC where voids and gas-filled cavities are observed according to the depth [14]. Experiments in Xe-implanted SiC are in progress.

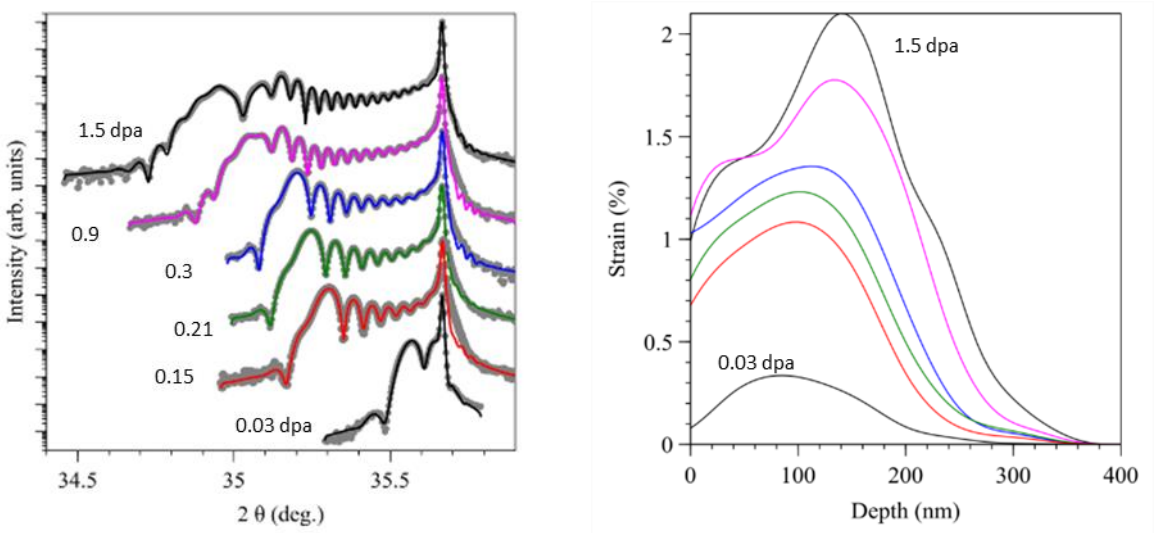

Figure 3. Evolution with increasing doses (0.03 to 1.5 dpa) of the experimental/simulated XRD curves (left) and the as-resulting strain profiles for SiC implanted with 540 keV xenon ions at 300°C (right).

4. Concluding remarks

Mechanisms for implantation-induced amorphization and strain build-up as function of temperature have been discussed. Above 300°C the amorphization is avoided and the strain distribution results from the contribution of three distinct accumulations of as-induced defects.

References

[1] Ziegler JF, Biersack JP and Ziegler MD 2008 *the Stopping Range In Matter*
[2] Jiang C, Daugault L, Audurier V, Tromas C, Declémy A, Beaufort MF and Barbot JF 2018 *Materials Today* **5** 14722
[3] Debelle A and Declémy A 2010 *Nucl. Inst. and Meth. B* **268** 1460
[4] Tyburska-Püschel B, Zhai Y, He L, Liu L, Boulle A, Voyles PM, Szlufarska I and Sridharan K 2016 *J. of Nucl. Mat*. **476** 132
[5] Souilah M, Boulle A and Debelle A 2016 *J. Appl. Cryst*. **49** 311.
[6] Leclerc S, Declémy A, Beaufort MF, Tromas C and Barbot JF 2005 *J. Appl. Phys*. **98** 113506
[7] Zhang Y, Weber WJ, Jiang W, Wang CM, Shutthanandan V and Hallen A 2004 *J. of Appl. Phys.* **95** 4012
[8] Weber WJ 2000 *Nucl. Inst. and Meth. B* **166-167** 98
[9] Weber WJ, Zhang Y and Wang L 2012 *Nucl. Inst. and Meth. B* **277** 1
[10] Friedland E 2004 *Nucl. Inst. and Meth. B* **217** 396
[11] Héliou R, Brebner JL and Roorda S 2001 *Semicond. Sci. Technol*. **16** 836.
[12] Zang H, Huo D, Shen T, He C, Wang Z, Pang L, Yao C and Yang T 2013 *J. Nucl. Mat* **433** 378
[13] Charaf Eddin A and Pizzagalli L 2012 *J. Nucl. Mat* **429** 329
[14] Zang H, Jiang W, Liu W, Deraraj A, Edwards DJ, Henager CH, Kurtz RJ, Li T, He C, Wang Z 2016 *Nucl. Inst. and Meth. B* **389-390** 40